

UC Irvine

UC Irvine Previously Published Works

Title

Red-Shifted Coumarin Luciferins for Improved Bioluminescence Imaging

Permalink

<https://escholarship.org/uc/item/3907d94k>

Journal

Journal of the American Chemical Society, 145(6)

ISSN

0002-7863

Authors

Love, Anna C

Caldwell, Donald R

Kolbaba-Kartchner, Bethany

et al.

Publication Date

2023-02-15

DOI

10.1021/jacs.2c07220

Peer reviewed



HHS Public Access

Author manuscript

J Am Chem Soc. Author manuscript; available in PMC 2024 February 15.

Published in final edited form as:

J Am Chem Soc. 2023 February 15; 145(6): 3335–3345. doi:10.1021/jacs.2c07220.

Red-Shifted Coumarin Luciferins for Improved Bioluminescence Imaging

Anna C. Love,

Department of Chemistry, University of California, Irvine, Irvine, California 92697, United States

Present Address: Center for Marine Biotechnology and Biomedicine, Scripps Institution of Oceanography, University of California, San Diego, California 92093, United States

Donald R. Caldwell,

Chemical Biology Laboratory, Cancer for Cancer Research, National Cancer Institute, National Institutes of Health, Frederick, Maryland 21702, United States

Bethany Kolbaba-Kartchner,

School of Molecular Sciences, Arizona State University, Tempe, Arizona 85281, United States

The Biodesign Center for Molecular Design and Biomimetics, Arizona State University, Tempe, Arizona 85281, United States

Katherine M. Townsend,

Department of Chemistry, University of California, Irvine, Irvine, California 92697, United States

Lila P. Halbers,

Department of Pharmaceutical Sciences, University of California, Irvine, Irvine, California 92697, United States

Zi Yao,

Department of Chemistry, University of California, Irvine, Irvine, California 92697, United States

Present Address: Department of Pharmaceutical Chemistry, University of California, San Francisco, California 94158, United States.

Caroline K. Brennan,

Department of Chemistry, University of California, Irvine, Irvine, California 92697, United States

Corresponding Authors: **Jeremy H. Mills** – School of Molecular Sciences, Arizona State University, Tempe, Arizona 85281, United States; The Biodesign Center for Molecular Design and Biomimetics, Arizona State University, Tempe, Arizona 85281, United States, jeremy.mills@asu.edu; **Martin J. Schnermann** – Chemical Biology Laboratory, Cancer for Cancer Research, National Cancer Institute, National Institutes of Health, Frederick, Maryland 21702, United States, martin.schnermann@nih.gov; **Jennifer A. Prescher** – Department of Chemistry, University of California, Irvine, Irvine, California 92697, United States; Department of Molecular Biology & Biochemistry and Department of Pharmaceutical Sciences, University of California, Irvine, Irvine, California 92697, United States, jpresche@uci.edu.

Author Contributions

All authors have given approval to the final version of the manuscript.

The authors declare the following competing financial interest(s): A provisional patent application on the bioluminescent probes has been filed.

ASSOCIATED CONTENT

Supporting Information

The Supporting Information is available free of charge at <https://pubs.acs.org/doi/10.1021/jacs.2c07220>.

Experimental details on luciferin synthesis, library development, analogue screens, and bioluminescence imaging are included (PDF)

Complete contact information is available at: <https://pubs.acs.org/doi/10.1021/jacs.2c07220>

Present Address: Chemical Research and Development, Pfizer Worldwide Research & Development, Groton, Connecticut 06340, United States

Joseph Ivanic,

Advanced Biomedical Computational Science, Frederick National Laboratory for Cancer Research, Leidos Biomedical Research, Inc., Frederick, Maryland 21702, United States

Tanya Hadjian,

Department of Chemistry, University of California, Irvine, Irvine, California 92697, United States

Jeremy H. Mills,

School of Molecular Sciences, Arizona State University, Tempe, Arizona 85281, United States

The Biodesign Center for Molecular Design and Biomimetics, Arizona State University, Tempe, Arizona 85281, United States

Martin J. Schnermann,

Chemical Biology Laboratory, Cancer for Cancer Research, National Cancer Institute, National Institutes of Health, Frederick, Maryland 21702, United States

Jennifer A. Prescher

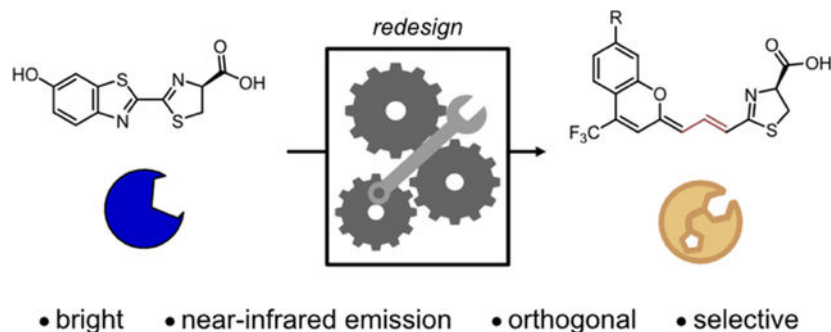
Department of Chemistry, University of California, Irvine, Irvine, California 92697, United States

Department of Molecular Biology & Biochemistry and Department of Pharmaceutical Sciences, University of California, Irvine, Irvine, California 92697, United States

Abstract

Multicomponent bioluminescence imaging *in vivo* requires an expanded collection of tissue-penetrant probes. Toward this end, we generated a new class of near-infrared (NIR) emitting coumarin luciferin analogues (CouLuc-3s). The scaffolds were easily accessed from commercially available dyes. Complementary mutant luciferases for the CouLuc-3 analogues were also identified. The brightest probes enabled sensitive imaging *in vivo*. The CouLuc-3 scaffolds are also orthogonal to popular bioluminescent reporters and can be used for multicomponent imaging applications. Collectively, this work showcases a new set of bioluminescent tools that can be readily implemented for multiplexed imaging in a variety of biological settings.

Graphical Abstract



INTRODUCTION

Bioluminescence imaging (BLI) features luciferase enzymes that oxidize luciferin small molecules to produce visible light.^{1–3} No external excitation source is required, so BLI enables sensitive imaging in preclinical models. Luciferase–luciferin pairs from the insect family in particular have been widely used for tracking cellular and molecular features *in vivo*.^{4–6} While popular, most of these reporters emit light that is readily absorbed and scattered by hemoglobin and other biomolecules.⁷

More tissue-penetrant light can be achieved with designer luciferase–luciferin pairs. These reporters comprise engineered substrates and enzymes capable of emitting near-infrared (NIR) light (Figure 1A).^{8–11} Such wavelengths are less susceptible to absorption and scatter and thus better suited for imaging in live animals. While NIR bioluminescent probes have been described, only a handful have been successfully deployed *in vivo*. Furthermore, most cannot be easily used in tandem for multiplexed imaging. BLI beyond two targets is not routine, as resolving multiple bioluminescent signals in tissues is challenging.^{12–14} Bioluminescent probes with NIR emission and unique, differentiable architectures would thus bolster efforts to visualize multicellular features in real time. Collections of such probes could provide new insights into tumor heterogeneity, immune cell behaviors, and other processes requiring the coordinated effort of multiple cell types.

Efforts to develop red-shifted pairs have focused on engineering the luciferase active site and luciferin small molecule. Early examples focused on modulating hydrogen-bond networks in the luciferin-binding pocket.^{15–17} Additional gains were made through synthetic manipulation of the small molecule.^{12,18–22} In fact, substantial redshifts in emission have been achieved with luciferins featuring pi-extended cores.^{8–11,23} One of the most well-known members of this class is AkaLumine, a vinyl luciferin analogue (Figure 1A).^{24,25} A complementary luciferase (Akaluc) for the pi-extended substrate was identified via extensive enzyme engineering.⁸ Akaluc/AkaLumine emits between 600 and 700 nm, wavelengths that are ~100 nm red-shifted from the parental truncated luciferin (comprising a single vinyl unit).⁸ Akaluc/AkaLumine has enabled deep tissue imaging in a variety of preclinical organisms, including marmosets.^{8,26–28}

Further shifts into the NIR region have been achieved with additional vinyl units^{29,30} and rigidified cores.^{9,31} In some cases, the resulting probe sets can be spectrally resolved from other bioluminescent reporters. For example, the NIR-emitting naphthyl luciferin NH₂-NpLH2 (Figure 1A)¹⁴ and its corresponding luciferase (CBR2) have been used for multiplexed imaging *in vivo* alongside a similarly engineered green-emitting variant. The different reporters were resolved via spectral unmixing.

While spectral differentiation is possible in some cases,^{2,32,33} many bioluminescent probes are difficult to discriminate *in vivo* via color alone. Luciferases typically exhibit broad, overlapping emission spectra that are challenging to resolve using conventional bioluminescence imagers (with surface read-outs).^{4,7} The depth of the luminescent probe also influences the signal intensity and emission profile registered at the detector. Deeper targets appear more “red” at the surface, which can confound spectral imaging.

An alternative approach to differentiating bioluminescent probes involves substrate resolution.^{11,23,34,35} Luciferases engineered to respond to unique molecules can be readily resolved via sequential application of their complementary luciferins. The majority of these orthogonal probe sets are suboptimal for imaging *in vivo*, though, as they give off <650 nm light. More distinct, red-emitting probes are thus necessary for facile multicomponent imaging in tissues.

To fill this void, we and others have focused on co-opting fluorophores with desirable photophysical properties (i.e., brightness, quantum yield, and emission profile) for luminophore development. In recent work, we introduced the CouLuc-1 analogues and their engineered luciferase, Pecan (Figure 1B).¹¹ The CouLuc-1 molecules comprise a novel class of red-emitting luciferins based on the trifluoromethyl coumarin structure.¹¹ The key trifluoromethyl group at C4 improves the quantum yield of such dyes and enhances charge separation in the excited state, resulting in red-shifted emission.^{36–41} This same modification is also known to improve the photostability of coumarin dyes.³⁸

Because CouLuc-1 analogues are small compared to other red-shifted luciferins, they were readily processed by a minimally modified Fluc variant (Pecan).³⁴ Only two mutations were required to achieve emission outputs comparable to the brightest red-shifted probe in the field, AkaLumine. By contrast, the complementary enzyme for AkaLumine (Akaluc) comprises 28 mutations that were identified over 21 rounds of screening.⁸ The unique architectures of the CouLuc-1 probes further enabled them to be used alongside Akaluc/AkaLumine and other state-of-the-art bioluminescent probes for multicomponent imaging.¹¹

We aimed to capitalize on the desirable features of the coumarin luciferins and extend their emission into the tissue-penetrant NIR region. Building on previous strategies, we surmised that extending the pi-conjugation by a single vinyl unit between the trifluoromethyl coumarin and the thiazoline ring would push emission from 595–630 to 695–730 nm (Figure 1B).^{9,24} This same two-carbon homologation logic has been used to generate the broadly used, and often multiplexed, indocyanine (“Cy”) fluorophore series.⁴² We further hypothesized that the additional vinyl modification could sufficiently differentiate the CouLuc-3 analogues from their CouLuc-1 counterparts, enabling multicomponent imaging via substrate resolution.

Here we report the design, synthesis, and application of NIR-emitting CouLuc-3 luminophores. We developed a concise four-to-six-step method to access the CouLuc-3 analogues. The luciferins exhibited ~100 nm red-shifted emission compared to the CouLuc-1 scaffolds, with $\lambda_{\text{max}}^{\text{EM}}$ values on par with the most red-shifted bioluminescent probes reported to date. Mutant luciferases capable of processing the elongated substrates were identified via Rosetta-guided enzyme engineering. The resulting luciferase–luciferin pairs exhibited robust emission *in cellulo* and *in vivo*. The CouLuc-3 analogues were further used alongside a collection of tissue-penetrant probes for facile, multiplexed imaging of tumor mimics. Collectively, this work expands the bioluminescent toolkit and sets the stage for future imaging studies of heterogeneous cell mixtures in tissues and whole organisms.

RESULTS AND DISCUSSION

Design and Synthesis of Pi-Extended Coumarin Luciferins.

We envisioned that additional vinyl groups bridging the coumarin and thiazoline units would substantially red-shift CouLuc emission into the near-infrared (NIR) regime. As noted earlier, AkaLumine exhibited a ~100 nm shift upon the addition of single vinyl unit from the parental scaffold.²⁴ We thus hypothesized that the CouLuc-3 molecules would exhibit ~100 nm redshifts relative to their single vinyl unit counterparts, placing their emission well within the NIR region (ca. 695–730 nm). While extended vinyl wires can degrade under laser illumination,^{43–45} bioluminescent probes are unique in that the luciferin excited state is protected in the luciferase active site. Thus, we anticipated that the CouLuc-3 analogues would enable robust imaging in cells and tissues.

We envisioned preparing the pi-extended CouLuc-3 analogues with different electron-donating groups (–NMe₂, –NH₂, –OH) on the coumarin heterocycle. The phenol group can be deprotonated in the light-emitting state, enabling red-shifted emission. Amino groups have also been used to red-shift luciferin emission.^{18,20} Amine substituents can further improve cell permeability.^{19,46} Indeed, the dimethylamino variant in the CouLuc-1 series demonstrated improved permeability over the phenolic analogue and the native substrate, D-luciferin. Structurally, the CouLuc-3 probes are comparable in size to both the naphthyl derivative NH₂-NpLH₂, and also AkaLumine.^{8,9} All three architectures (CouLuc-3, AkaLumine, NH₂-NpLH₂) have a 12-atom distance from the carbon of the carboxylic acid to the carbon bearing the electron-donating group. Thus, we anticipated engineering a mutant enzyme to accept these substrates would be feasible.

The synthesis of the CouLuc-3 series builds on our prior work to assemble CouLuc-1 derivatives (Scheme 1). We previously found that cyanomethylene compounds, including the dimethyl aniline **1a**, could be accessed through the addition of cyanomethyl anions to commercially available coumarins followed by acid-promoted elimination.¹¹ Conversion of **1a** to the CouLuc-3 variant required the introduction of an ethylene unit, which we were able to efficiently implement. Compound **1a** underwent DIBAL reduction to aldehyde **2a**, followed by Wittig reaction with (cyanomethylene)triphenylphosphorane to form the corresponding unsaturated nitrile **3a**. Final condensation of **3a** (as a mixture of isomers) with D-cysteine and NaHCO₃ in degassed ethanol (72 h) provided **CouLuc-3-NMe₂** as a single isomer.

We then set out to prepare **CouLuc-3-NH₂** and **CouLuc-3-OH**. We found that the aniline and phenol groups were incompatible with the DIBAL reduction/Wittig sequence (Figure S1A). After examining several aniline-protecting group candidates (Figure S1B), we ultimately found the diallyl aniline **1b** could undergo reduction to form aldehyde **2b**, Wittig olefination to form **3b**, deprotection to form **3c**, and cysteine condensation to provide **CouLuc-3-NH₂**. Similarly, benzyl ether **1c** underwent the reduction, Wittig, deprotection sequence to form **3e**, followed by final cysteine condensation to provide **CouLuc-3-OH** (Figure S1C). In both of these sequences, the intermediate nitriles and aldehydes were accessed as mixtures of olefin isomers, whereas the final compounds were single isomers.

We then examined the structure and spectroscopic properties of the series of compounds. The geometries of **CouLuc-3-NMe₂** and **CouLuc-3-OH** were assigned using two-dimensional nuclear Overhauser effect spectroscopy (2D NOESY) (Figures S2 and S3). Since a single product emerges from a mixture of olefin isomers, we hypothesized that the condensation might be thermodynamically controlled. Computational analysis of the phenol variant revealed that the observed structure is preferred by 1–4 kcal/mol over the energetically nearest olefin isomers. The thiazole ring is predicted to favor the *s*-cis form over *s*-trans, by 0.2 kcal/mol, but both are comparable (Figure S4). We also measured the absorbance and fluorescence properties of the analogues in various organic solvents and buffers (Figure S5 and Table S1). The CouLuc-3 probes were red-shifted from their CouLuc-1 counterparts, underscoring their potential for sensitive bioluminescence imaging.

***In Vitro* Characterization of CouLuc-3 Bioluminescence.**

With the CouLuc-3 luciferins in hand, we measured photon outputs with native Fluc. All analogues produced light, with **CouLuc-3-OH** emitting more brightly than either amino analogue (Figure S6A). This result was surprising, as the hydroxy variant was the dimmest compound in the previously reported CouLuc-1 series.¹¹ We hypothesized that the larger amino appendages in the CouLuc-3 panel engendered a steric clash with Fluc, resulting in poorer emission (Figure S6A). All analogues provided weaker outputs compared to the native substrate, D-luciferin (D-luc), producing ca. 1000- to 50,000-fold fewer photons overall.

While the two amino analogues were too dim to measure bioluminescence spectra, we found that Fluc/**CouLuc-3-OH** emitted maximally at 730 nm (Figure S7). This output is on par with the most red-shifted luciferin analogues reported to date.⁹ Interestingly, the fluorescence emission of **CouLuc-3-OH** in phosphate-buffered saline (PBS, pH 7.4) was ~50 nm blue-shifted from the observed BLI emission with Fluc (Figure S5). However, the fluorescence emission maximum in dimethylformamide (DMF) matched that of the bioluminescence spectrum (730 nm). Similar solvatochromatic behavior was observed with the **CouLuc-3-NMe₂** analogue (Figure S5 and Table S1). Building on these findings, we hypothesized that subtle changes in the polarity of the luciferase active site could influence the emission maxima and potentially red-shift emission even further.

Rosetta-Guided Design of Mutant Luciferases.

We aimed to identify more robust luciferase/CouLuc-3 pairs. Ideally, these pairs would also be orthogonal to existing state-of-the-art, red-shifted BLI probes to enable sensitive multi-component imaging. We used the RosettaMatch and RosettaDesign algorithms to guide our approach;^{47–49} both of these methods have been used previously to identify starting points for luciferase engineering.^{11,23} Such approaches are also critical to guide mutagenesis efforts in the absence of light emission (as was the case for the amino CouLuc-3 analogues). We first used the RosettaMatch algorithm⁴⁸ to dock each luciferin analogue within a firefly luciferase structure (Fluc, PDB ID: 4g36) in a native-like orientation. The RosettaDesign algorithm⁴⁹ was then used to randomly mutate residues in the vicinity of the docked luciferin analogue. During the design calculations, each mutation was analyzed using the Rosetta energy function.⁵⁰ Mutations that decrease the Rosetta energy are often

suggestive of the alleviation of clashes between native residues and the novel luciferins, or the introduction of productive interactions (e.g., hydrogen bonds or hydrophobic packing interactions) with the new substrate. When used in this way, Rosetta can restructure the active site to accommodate structural misfits.

We selected **CouLuc-3-OH** and **CouLuc-3-NMe₂** to guide the initial designs and overall engineering campaign (Figure 2A). **CouLuc-3-OH** bears an electron-donating group with a pK_a near physiological pH. Screening data from this compound would thus provide insight into how active site polarity affects emission wavelength. Screening data from the most sterically demanding analogue, **CouLuc-3-NMe₂**, would likely provide insight into complementary luciferases for a range of other CouLuc-3 analogues, including **CouLuc-3-NH₂**.

CouLuc-3-NMe₂ and **CouLuc-3-OH** were subjected to a Rosetta workflow similar to our previous study.¹¹ The algorithm found a significant steric clash between the side chain of R218 and the electron-donating group of the CouLuc-3 luciferins (Figure 2B). Interestingly, R218 luciferase mutants were previously shown to improve the binding of sterically modified D-luc analogues.^{13,34} Prior work also showed that an R218K mutant provides improved photon output and red-shifted emission with amino luciferin analogues.^{15,20} While no other significant active site clashes were observed, Rosetta suggested 40 additional sites for mutation across the Fluc active site and AMP-binding domain. Mutations in the AMP-binding domain have been found to greatly reduce activity with the native substrate, and in some cases, boost red-shifted emission with synthetic substrates.¹⁰ Thus, several Rosetta-suggested sites from the AMP-binding domain were included in library development. In total, 20 of the 41 suggested mutations were initially targeted to design and screen a library (Tables S2 and S3).

Identifying Complementary Luciferase Mutants for CouLuc-3 Analogues.

The initial Rosetta-inspired library was subjected to an established screening workflow (Figure S8).¹¹ From ~16,000 colonies screened on plate, 107 reproducibly emitted 10-fold more photons than Fluc with the CouLuc-3 analogues (Figure S9). The majority of the luciferase hits comprised mutations at position 218. These mutations likely create space for the elongated structures as predicted by Rosetta analysis. Other frequently mutated sites among the generation 1 hits included H221 (33% mutated), N229 (14% mutated), and A222 (11% mutated, Figure 2C). The top six mutants were further isolated to confirm light output (Figure 2D). While large improvements in emission were observed, overall photon outputs were below the target threshold of established red-emitting probe sets in the field (e.g., Akaluc/AkaLumine). Thus, three clones were carried forward for additional mutagenesis and screening.

The second-generation library preserved mutations from generation 1 hits while targeting other Rosetta-predicted “hot spots”. The hot spots comprised residues (e.g., H221 and A222) that were frequently mutated in generation 1 hits but were unmodified in the brightest-emitting clones. For example, mutations at H221 and A222 were not present in the top 3 hits from generation 1, but comprised 33 and 11%, respectively, of the remaining 107 hits. H221 and A222, along with 18 other sites, were randomized in the generation 2 library. The

library was screened as above, but no hits were identified (upon screening ~8000 colonies) that provided enhanced photon outputs over the generation 1 hits (Figure 2E).

To explore additional sequence space, we used RosettaDesign to predict new sites to target. Energy-minimized models of CouLuc-3 analogues bound to the top three generation 1 hits were produced. Many of the sites implicated in luciferin processing were similar to those identified in the generation 1 screen. Some new sites were uncovered, though, including E311. This residue caught our attention, as E311 mutations were previously shown to enhance the turnover of other pi-extended luciferins.²³ Additional sites to target were determined empirically via screening against an established library of functional luciferase mutants (Figure S10).³⁴ This library contained Pecan, the complementary luciferase for CouLuc-1 probes. Screening with the CouLuc-3 derivatives revealed positions E311, Y255, and F260 as potential targets for mutagenesis (Figure S10). Based on these empirical screens and Rosetta analyses, 15 additional sites were selected for a third-generation library.

The generation 3 library was constructed and screened with the CouLuc-3 analogues (Tables S4 and S5, Figures 2E and S11). On-plate analyses of ~6,000 colonies revealed a divergence in enzyme preference for the amino and hydroxy variants (Figure S11). Enzymes bearing a mutation at position 260 generally emitted brightly with **CouLuc-3-NMe₂**, while enzymes bearing mutations at positions 219 and 255 generally emitted brightly with **CouLuc-3-OH**. Among these hits, two standouts were identified: mutant 709 (which emitted brightly with **CouLuc-3-OH**) and mutant 1023 (which emitted brightly with **CouLuc-3-NMe₂**).

We continued the enzyme engineering campaign with mutants 709 and 1023, to achieve brighter photon outputs. A fourth-generation library was prepared using Rosetta-guided approaches, in combination with random mutagenesis via error-prone polymerase chain reaction (PCR) (Figure S12).⁵¹ However, no further improvements in light output were achieved. We then generated a shuffled library, in which six residues identified in the previous screens were randomized. Three of the targeted residues originated from the generation 1 screen (R218, H221, N229), and three were from the generation 3 screen (Y255, F260, E311). The library was constructed using gene assembly with mutagenic primers (Table S6). Screening was performed (~36,000 colonies) with the CouLuc-3 analogues, but no mutants with photon outputs higher than 709/1023 were identified. In fact, the top hits (58%) with **CouLuc-3-NMe₂** comprised the same amino acid sequence as mutant 1023 (Figure S13A). We further identified a top-performing mutant for **CouLuc-3-OH** that possessed the same sequence as mutant 709 (Figure S13A). Docking analyses with energy-minimized mutants confirmed that the active site architectures of mutants 709 and 1023 are uniquely suited for CouLuc-3 processing (Figure S14). Further, the mutants provided robust photon outputs with their matched CouLuc-3 analogues in bacterial lysate. Thus, we moved forward with these mutants, naming 1023, Pistachio (Figures 2E and 3B).

Characterization of CouLuc-3 Analogues with Mutant Luciferase Hits.

We further characterized the mutant luciferase hits and assessed their potential for *in vivo* imaging with CouLuc-3 analogues (Figures 3A,B and S15). When **CouLuc-3-NMe₂** and **CouLuc-3-NH₂** were incubated with recombinant Pistachio, robust light emission was observed (380-fold and 92-fold improvement compared to CouLuc-3 analogues incubated

with Fluc). The large gains in photon output were due to the lack of CouLuc-3 turnover by Fluc (likely due to steric occlusion, as noted earlier). Minimal-to-no photon output above background was observed for either amino CouLuc-3 compound upon incubation with Fluc. Kinetic analyses verified that the CouLuc-3 analogues bind their respective mutant hits with relatively high affinity (Figures 3C and S16). High nanomolar to low micromolar K_m values were measured, on par with other pi-extended synthetic luciferin analogues (AkaLumine, NH₂-NpLH2) and their complementary mutants.^{8,9} The nonpolar nature of the CouLuc-3 analogues coupled with the more hydrophobic mutations of the enzymes likely drive the enhanced affinity.

The engineered luciferase–luciferin pairs provided red-shifted emission. The amino CouLuc-3 analogues emitted maximally between 710 and 730 nm (96–99% of photons >650 nm) with their matched enzymes (Figure 3D). The emission profiles are ~100 nm red-shifted from the respective CouLuc-1 probes. The peak emission values are also on par with the most widely used red-shifted bioluminescent probes reported to date (NH₂-NpLH2/CBR2, Akaluc/AkaLumine). No substantial differences in emission were observed when the amino CouLuc-3 analogues were incubated with mutant 709 versus Pistachio. By contrast, the emission spectrum for **CouLuc-3-OH** changed considerably between Pistachio and mutant 709 (Figure S17A). **CouLuc-3-OH** exhibited a similar degree of red-shifted emission as the amino variants (99% of photons >650 nm) with mutant 709. However, with Pistachio, the emission spectrum was bimodal, with local maxima at 665 nm and 710 nm, reducing the overall percentage of tissue-penetrant photons (Figure S17A). These results suggest that subtle changes to the luciferase active site architecture and polarity can preferentially stabilize different emitters (e.g., different protonation states of **CouLuc-3-OH**).

Pistachio and mutant 709 differ only slightly in terms of their primary sequence (Figure 3B). Notably, though, Pistachio contains an H221I mutation. Residues near position 221 have been implicated in structuring a water cluster found in the active site.^{15,17,52–54} This cluster can impact the conformation and protonation state of the excited state emitter, which in turn, influence the color of light produced. Changes to luciferase residues can further modulate the local pH.^{17,53–55} We therefore hypothesized that the change from histidine bearing a polar, charged side chain, to isoleucine bearing a nonpolar and uncharged side chain, could influence the protonation state of **CouLuc-3-OH** (Figure S17).

To test the hypothesis, we installed an H221I mutation in mutant 709. When this mutant was treated with **CouLuc-3-OH**, a shoulder of blue-shifted emission (665 nm) was revealed by bioluminescence spectroscopy. Based on pK_a values for related hydroxycoumarin scaffolds,⁵⁶ we expected the emissive luminophore to be predominantly the phenol at pH values <8 and the phenolate at pH values >8. The phenolate species, in the case of D-luc, emits red-shifted light compared to the phenol.⁵⁷ Bioluminescence spectra were recorded for mutant 709(H221I) and **CouLuc-3-OH** over a range of pH values. As the pH decreased, the ratio of photons at 730 nm (attributed to the phenolate) versus 665 nm (attributed to the phenol) also decreased (Figure S18A). The high noise in the spectra at pH values below 7 and above 8 was attributed to decreased activity of the enzyme and thus reduced overall light emission.⁵⁸ As the pH increased, the shoulder disappeared, and λ_{\max}^{EM} increased.

Collectively, these data suggest that H221 influences the local pH, promoting emission from the phenolate form of the CouLuc-3 analogue.

A similar trend in pH-dependent emission was observed when Pistachio was incubated with **CouLuc-3-OH** (Figure S18B). However, the percentage of photons emitting <650 nm remained larger at higher pH values than for the 709(H221I) point mutant. While both Pistachio and 709 bear R218 mutations, the residues are distinct (Ser for Pistachio, Val for 709). The resulting difference in polarity could influence the binding mode and contribute to the more blue-shifted emission observed in Pistachio even at high pH values.¹⁷

Imaging *in Cellulo* with CouLuc-3 Analogues.

We next evaluated the CouLuc-3 analogues and mutant luciferases in mammalian cells. The top hits identified from screening were transiently expressed in HEK293 cells. The cells were then incubated with either CouLuc-3 analogues or D-luc. Excitingly, when Pistachio-expressing cells were incubated with **CouLuc-3-NMe₂**, emission was significantly brighter than **CouLuc-3-NMe₂** incubated with Fluc-expressing cells. This fold induction is notable because very few luciferase mutations were required to achieve robust output. Similar fold improvements were observed with the other CouLuc-3 analogues (Figures 3E and S19).

The Pistachio/**CouLuc-3-NMe₂** pair provided photon outputs on par with Fluc/D-luc in HEK293 cells. The compound was also well tolerated by cells at the doses used for imaging (Figure S20). The Pistachio/**CouLuc-3-NMe₂** pair further emitted significant numbers of NIR photons in cells (Figure S21), suggesting that the duo would be suitable for *in vivo* imaging.

Tissue and *In Vivo* Imaging with Pistachio/CouLuc-3-NMe₂.

To showcase the new red-shifted probes for tissue and *in vivo* imaging, we generated cancer cell lines (4T1 and JIMT-1) stably expressing Pistachio and other luciferase reporters. When the cells were incubated with **CouLuc-3-NMe₂**, reduced levels of light output were observed compared to HEK293 cell studies. This result was likely due to lower expression levels of the luciferase reporters and reduced compound transport (Figure S22). Photon emission was sufficiently bright and red-shifted, though, for further application in tissues (Figure S22B,D). To demonstrate, luciferase-expressing 4T1 or JIMT-1 cells were plated under tissue slices (turkey bacon, 1 mm per slice) and the matching luciferins were supplied. Pistachio/**CouLuc-3-NMe₂** outperformed Fluc/D-luc and Akaluc/AkaLumine in terms of the percentage of tissue-penetrant photons produced (Figure 4A,B).

Pistachio/**CouLuc-3-NMe₂** was further evaluated *in vivo* alongside Fluc/D-luc and Akaluc/AkaLumine. JIMT-1 luciferase-expressing cells were implanted subcutaneously in each flank of 6-week-old female NU/NU mice and allowed to grow for 6 days prior to imaging. Equimolar amounts of substrate were administered to the animals *via* intraperitoneal (i.p.) injection, and images were acquired. Bright emission was observed for mice treated with Pistachio/**CouLuc-3-NMe₂** and Fluc/D-luc (Figures S23 and S24). Adverse effects were observed in mice treated with AkaLumine, similar to other reports.^{59–61} In our case, the mice seized shortly after substrate injection and anesthetization. It is possible that

these effects were related to disrupted cardiac function,⁶⁰ but follow-up studies were not performed. Pistachio/**CouLuc-3-NMe₂** produced light on par with emission from Fluc/D-luciferin, despite the latter probe set emitting an order of magnitude more photons *in cellulo* (Figures S22A and S23B). The gains *in vivo* were likely due to the red-shifted emission of Pistachio/**CouLuc-3-NMe₂**.

The time needed to reach maximum emission with Pistachio/**CouLuc-3-NMe₂** in the experiment (2 h post injection, Figure S23C) was substantially longer than the time needed to reach peak emission for Fluc (25 min post injection). These data suggest that **CouLuc-3-NMe₂** is less bioavailable *in vivo*, offsetting the gains in sensitivity achieved from red light emission. We hypothesized that photon outputs from Pistachio/**CouLuc-3-NMe₂** could be enhanced with alternative delivery vehicles. Indeed, improvements in emission were achieved at earlier time points when **CouLuc-3-NMe₂** was delivered i.p. using established formulations⁶² (Figure S25).

The red-shifted emission of Pistachio/**CouLuc-3-NMe₂** is arguably most beneficial for imaging small numbers of cells in opaque environments. To showcase the pair in this context, Pistachio-expressing JIMT-1 cells were implanted in mice with intact black fur. Upon formulated **CouLuc-3-NMe₂** injection, Pistachio-expressing tumors exhibited slightly stronger light outputs compared to Fluc-expressing tumors (treated with D-luc, Figure 4C,D). Peak emission for the Pistachio/**CouLuc-3-NMe₂** pair was again observed only hours after compound injection (Figure S26), suggesting reduced bioavailability of the luciferin substrate. Additional improvements can likely be achieved with optimized delivery vectors and/or administration modes, and work along these lines is ongoing.

Multicomponent Imaging *in Cellulo* with Pistachio.

The unique architecture of the CouLuc-3 analogues makes them well suited for multicomponent imaging both *in vitro* and *in vivo*. We surmised that they could even be used in tandem with CouLuc-1 analogues, which are preferentially processed by the mutant enzyme Pecan, bearing mutations at S347 and F243. Pecan retains a key residue (R218) that precludes CouLuc-3 binding; this residue is mutated in Pistachio to enable CouLuc-3 processing. To test whether the probes could be used for multicomponent imaging, we combined five different luciferase-expressing JIMT-1 cell lines and added the corresponding substrates. Each substrate was added in sequence and images were acquired after substrate addition (Figure 5A). The raw images were processed using a linear unmixing algorithm to deconvolute signals produced from each pair.⁶³ As shown in Figure 5B, robust orthogonality was observed within this quintet set.

To showcase the utility of orthogonal imaging with Pistachio/**CouLuc-3-NMe₂**, we examined an established heterogeneous breast tumor model. The cell lines derived from a spontaneously metastatic mouse breast tumor (i.e., 4T1, 4T07, and 66cl4 cell lines).⁶⁴ Cellular heterogeneity has been implicated in the evolution toward drug resistance in cancer and can potentiate tumorigenicity.^{65–68} A better understanding of how multicellular interactions impact growth rate and other features would bolster our understanding of cancer and other diseases. Toward this end, each cell line was engineered to express a unique,

orthogonal luciferase. The cells were plated as mixtures in defined regions (“mixed”) or separated, but allowed to share media (“separate,” Figure 5C). Control samples comprised single populations of luciferase-expressing cells grown in isolation. We assayed cells for light emission over three days post-plating and used the change in total photon flux as an indicator of proliferation. In separate conditions, cell growth matched the growth observed from control plates. However, in mixed conditions, stark differences in proliferation were observed. 4T07 and 4T1 cells showed higher levels of growth while 66cl4 cells showed slightly decreased levels of growth compared to control plates (Figures 5D and S27). These data demonstrate how expanded sets of bioluminescent probes can begin to disentangle complex biological processes involving heterogeneous cell populations.

CONCLUSIONS

Despite the growing toolbox of bioluminescent probes, there remain only a handful with both bright and red-shifted emission (>700 nm). We addressed the need for additional NIR-emitting probes by developing and characterizing a panel of new coumarin luciferins. The analogues were synthesized in four to six steps, and complementary mutant luciferases were identified via enzyme engineering. The brightest pair, Pistachio/**CouLuc-3-NMe₂** exhibited photon outputs on par with native bioluminescent systems *in vitro* and in cells. The pair also provided red-shifted light on par with the most tissue-penetrant probes reported to date.

When applied *in vivo*, Pistachio/**CouLuc-3-NMe₂** exhibited robust photon outputs analogous to the native Fluc/D-luc system. Imaging in mice with intact black fur, an often challenging environment, was further possible. The gains in red-shifted emission in this context, though, were offset by suboptimal bioavailability. Several hours were needed to achieve peak emission with the CouLuc-3 probe, and the maximum light output achieved was only on par with Fluc/D-luc. Additional work is thus necessary to realize the full potential of the probe set for imaging *in vivo*. Further improvements are expected with alternative formulations or delivery mechanisms, and studies along these lines are underway. We also plan to examine **CouLuc-3-NMe₂** longevity in various tissues. It is possible that the probe is metabolized or otherwise degraded *in vivo*, reducing the effective overall dose in certain environments.

The unique chemical space occupied by the CouLuc-3 probes further enabled multicomponent imaging with up to five luciferase species in cells. We leveraged their orthogonality to examine how heterogeneous mixtures influence cancer cell proliferation. These results set the stage for future investigations into clinically relevant heterogeneous tumor behavior *in vivo*. Future work will also focus on additional modifications to the luciferin scaffold, accessing substrates capable of >800 nm emission.

Supplementary Material

Refer to Web version on PubMed Central for supplementary material.

ACKNOWLEDGMENTS

This work was supported by the U.S. National Institutes of Health (R01 GM107630 to J.A.P.) and the Intramural Research Program of the National Institutes of Health (NIH), NCI-CCR. This project has been further supported with Federal funds from the National Cancer Institute, National Institutes of Health, under Contract No. HHSN261200800001E. A.C.L. was supported by the National Science Foundation *via* the BEST IGERT (DGE-1144901) program. The authors thank the Barbara Karamos Cancer Center for contributing the 4T1, 4T07, and 66Cl4 cancer cell lines, and the NIH NCI-CCR for contributing the JIMT-1 cells. Some experiments were performed at the Laser Spectroscopy labs (LSL) at UCI. The authors thank Dr. Joseph Barchi, NCI-CCR, for NMR assistance and Dr. James Kelley, NCI-CCR, for mass spectrometric analysis. The authors also thank Dr. Jennifer Atwood for performing cell sorting on generated stable cell lines. They acknowledge the support of the Chao Family Comprehensive Cancer Center IFI Flow Cytometry Core Shared Resource, supported by the National Cancer Institute of the National Institutes of Health under award number P30CA062203. Additional thanks to the members of the Prescher lab for helpful discussions, along with members of the Weiss and Martin laboratories for providing equipment and reagents.

REFERENCES

- (1). Kaskova ZM; Tsarkova AS; Yampolsky IV 1001 Lights: luciferins, luciferases, their mechanisms of action and applications in chemical analysis, biology and medicine. *Chem. Soc. Rev.* 2016, 45, 6048–6077. [PubMed: 27711774]
- (2). Mezzanotte L; van 't Root M; Karatas H; Goun EA; Löwik CWGM In Vivo Molecular Bioluminescence Imaging: New Tools and Applications. *Trends Biotechnol.* 2017, 35, 640–652. [PubMed: 28501458]
- (3). Zambito G; Chawda C; Mezzanotte L Emerging tools for bioluminescence imaging. *Curr. Opin. Chem. Biol.* 2021, 63, 86–94. [PubMed: 33770744]
- (4). Contag CH; Bachmann MH Advances in *in vivo* bioluminescence imaging of gene expression. *Annu. Rev. Biomed. Eng.* 2002, 4, 235–260. [PubMed: 12117758]
- (5). Prescher JA; Contag CH Guided by the light: visualizing biomolecular processes in living animals with bioluminescence. *Curr. Opin. Chem. Biol.* 2010, 14, 80–89. [PubMed: 19962933]
- (6). Contag CH *In vivo* pathology: seeing with molecular specificity and cellular resolution in the living body. *Annu. Rev. Pathol. Mech. Dis.* 2007, 2, 277–305.
- (7). Zhao H; Doyle TC; Coquoz O; Kalish F; Rice BW; Contag CH Emission spectra of bioluminescent reporters and interaction with mammalian tissue determine the sensitivity of detection *in vivo*. *J. Biomed. Opt.* 2005, 10, No. 041210.
- (8). Iwano S; Sugiyama M; Hama H; Watakabe A; Hasegawa N; Kuchimaru T; Tanaka KZ; Takahashi M; Ishida Y; Hata J; Shimozone S; Namiki K; Fukano T; Kiyama M; Okano H; Kizaka-Kondoh S; McHugh TJ; Yamamori T; Hioki H; Maki S; Miyawaki A Single-cell bioluminescence imaging of deep tissue in freely moving animals. *Science* 2018, 359, 935. [PubMed: 29472486]
- (9). Hall MP; Woodroffe CC; Wood MG; Que I; van't Root M; Ridwan Y; Shi C; Kirkland TA; Encell LP; Wood KV; Löwik C; Mezzanotte L Click beetle luciferase mutant and near infrared naphthyl-luciferins for improved bioluminescence imaging. *Nat. Commun.* 2018, 9, No. 132. [PubMed: 29317625]
- (10). Stowe CL; Burley TA; Allan H; Vinci M; Kramer-Marek G; Ciobota DM; Parkinson GN; Southworth TL; Agliardi G; Hotblack A; Lythgoe MF; Branchini BR; Kalber TL; Anderson JC; Pule MA Near-infrared dual bioluminescence imaging in mouse models of cancer using infraluciferin. *eLife* 2019, 8, No. e45801. [PubMed: 31610848]
- (11). Yao Z; Caldwell DR; Love AC; Kolbaba-Kartchner B; Mills JH; Schnermann MJ; Prescher JA Coumarin luciferins and mutant luciferases for robust multi-component bioluminescence imaging. *Chem. Sci.* 2021, 12, 11684–11691. [PubMed: 34659703]
- (12). Evans MS; Chaurrette JP; Adams ST; Reddy GR; Paley MA; Aronin N; Prescher JA; Miller SC A synthetic luciferin improves bioluminescence imaging in live mice. *Nat. Methods* 2014, 11, 393–395. [PubMed: 24509630]
- (13). Rathbun CM; Porterfield WB; Jones KA; Sagoe MJ; Reyes MR; Hua CT; Prescher JA Parallel screening for rapid identification of orthogonal bioluminescent tools. *ACS Cent. Sci.* 2017, 3, 1254–1261. [PubMed: 29296665]

- (14). Zambito G; Hall MP; Wood MG; Gaspar N; Ridwan Y; Stellari FF; Shi C; Kirkland TA; Encell LP; Löwik C; Mezzanotte L Red-shifted click beetle luciferase mutant expands the multicolor bioluminescent palette for deep tissue imaging. *iScience* 2021, 24, No. 101986. [PubMed: 33490896]
- (15). Branchini BR; Magyar RA; Murtiashaw MH; Portier NC The role of active site residue arginine 218 in firefly luciferase bioluminescence. *Biochemistry* 2001, 40, 2410–2418. [PubMed: 11327861]
- (16). Ugarova NN; Brovko LY Protein structure and bioluminescent spectra for firefly bioluminescence. *Luminescence* 2002, 17, 321–330. [PubMed: 12407671]
- (17). Branchini BR; Magyar RA; Murtiashaw MH; Anderson SM; Helgerson LC; Zimmer M Site-directed mutagenesis of firefly luciferase active site amino acids: a proposed model for bioluminescence color. *Biochemistry* 1999, 38, 13223–13230. [PubMed: 10529195]
- (18). Reddy GR; Thompson WC; Miller SC Robust light emission from cyclic alkylaminoluciferin substrates for firefly luciferase. *J. Am. Chem. Soc.* 2010, 132, 13586–13587. [PubMed: 20828122]
- (19). Harwood KR; Mofford DM; Reddy GR; Miller SC Identification of mutant firefly luciferases that efficiently utilize aminoluciferins. *Chem. Biol.* 2011, 18, 1649–1657. [PubMed: 22195567]
- (20). Mofford DM; Reddy GR; Miller SC Aminoluciferins extend firefly luciferase bioluminescence into the near-infrared and can be preferred substrates over D-luciferin. *J. Am. Chem. Soc.* 2014, 136, 13277–13282. [PubMed: 25208457]
- (21). Adams ST; Miller SC Beyond D-luciferin: expanding the scope of bioluminescence imaging *in vivo*. *Curr. Opin. Chem. Biol.* 2014, 21, 112–120. [PubMed: 25078002]
- (22). Sharma DK; Adams ST; Liebmann KL; Choi A; Miller SC Sulfonamides are an overlooked class of electron donors in luminogenic luciferins and fluorescent dyes. *Org. Lett.* 2019, 21, 1641–1644. [PubMed: 30835125]
- (23). Yao Z; Zhang BS; Steinhardt RC; Mills JH; Prescher JA Multicomponent bioluminescence imaging with a π -extended luciferin. *J. Am. Chem. Soc.* 2020, 142, 14080–14089. [PubMed: 32787261]
- (24). Iwano S; Obata R; Miura C; Kiyama M; Hama K; Nakamura M; Amano Y; Kojima S; Hirano T; Maki S; Niwa H Development of simple firefly luciferin analogs emitting blue, green, red, and near-infrared biological window light. *Tetrahedron* 2013, 69, 3847–3856.
- (25). Kuchimaru T; Iwano S; Kiyama M; Mitsumata S; Kadonosono T; Niwa H; Maki S; Kizaka-Kondoh S A luciferin analogue generating near-infrared bioluminescence achieves highly sensitive deep-tissue imaging. *Nat. Commun.* 2016, 7, No. 11856. [PubMed: 27297211]
- (26). Guo Y; Wang B; Chen Y; Liang M; Wang H; Wang C; Liang H; Zhou Y; Xi J; Ci L; Sun R; Fei J; Shen R A bioluminescence reporter mouse strain for *in vivo* imaging of CD8⁺ T cell localization and function. *Biochem. Biophys. Res. Commun.* 2021, 581, 12–19. [PubMed: 34653673]
- (27). Zhou M; Xing Q; Zhang D; Zhang C; Zhang Y; Zhang J; Shan Y Generation of an Akaluc knock-in human embryonic stem cell reporter line using CRISPR-Cas9 technology. *Stem Cell Res.* 2021, 56, No. 102532. [PubMed: 34509917]
- (28). Takagi S; Sasaki Y; Koike S; Takemoto A; Seto Y; Haraguchi M; Ukaji T; Kawaguchi T; Sugawara M; Saito M; Funouchi Y; Ae K; Matsumoto S; Fujita N; Katayama R Platelet-derived lysophosphatidic acid mediated LPAR1 activation as a therapeutic target for osteosarcoma metastasis. *Oncogene* 2021, 40, 5548–5558. [PubMed: 34302117]
- (29). Kamiya G; Kitada N; Saito-Moriya R; Obata R; Iwano S; Miyawaki A; Hirano T; Maki SA Development of phenyl oligoene-type firefly luciferin analogues with extended π -electronic conjugation for near-infrared bioluminescence. *Chem. Lett.* 2021, 50, 1523–1525.
- (30). Saito R; Kuchimaru T; Higashi S; Lu SW; Kiyama M; Iwano S; Obata R; Hirano T; Kizaka-Kondoh S; Maki SA Synthesis and luminescence properties of near-infrared *N*-heterocyclic luciferin analogues for *in vivo* optical imaging. *Bull. Chem. Soc. Jpn.* 2019, 92, 608–618.
- (31). Ikeda Y; Nomoto T; Hiruta Y; Nishiyama N; Citterio D Ring-fused firefly luciferin: expanded palette of near-infrared emitting bioluminescent substrates. *Anal. Chem.* 2020, 92, 4235–4243. [PubMed: 31971368]

- (32). Mezzanotte L; Que I; Kaijzel E; Branchini B; Roda A; Löwik C Sensitive dual color *in vivo* bioluminescence imaging using a new red codon optimized firefly luciferase and a green click beetle luciferase. *PLoS One* 2011, 6, No. e19277. [PubMed: 21544210]
- (33). Zambito G; Gaspar N; Ridwan Y; Hall MP; Shi C; Kirkland TA; Encell LP; Löwik C; Mezzanotte L Evaluating brightness and spectral properties of click beetle and firefly luciferases using luciferin analogues: identification of preferred pairings of luciferase and substrate for *in vivo* bioluminescence imaging. *Mol. Imaging Biol.* 2020, 22, 1523–1531. [PubMed: 32926287]
- (34). Jones KA; Porterfield WB; Rathbun CM; McCutcheon DC; Paley MA; Prescher JA Orthogonal luciferase–luciferin pairs for bioluminescence imaging. *J. Am. Chem. Soc.* 2017, 139, 2351–2358. [PubMed: 28106389]
- (35). Williams SJ; Prescher JA Building biological flashlights: orthogonal luciferases and luciferins for *in vivo* imaging. *Acc. Chem. Res.* 2019, 52, 3039–3050. [PubMed: 31593431]
- (36). Sun W-C; Gee KR; Haugland RP Synthesis of novel fluorinated coumarins: Excellent UV-light excitable fluorescent dyes. *Bioorg. Med. Chem. Lett.* 1998, 8, 3107–3110. [PubMed: 9873685]
- (37). Taneja L; Sharma AK; Singh RD Study of photophysical properties of coumarins: substituent and concentration dependence. *J. Lumin.* 1995, 63, 203–214.
- (38). Fletcher AN; Bliss DE Laser dye stability. Part 5. *Appl. Phys.* 1978, 16, 289–295.
- (39). Gandioso A; Bresolí-Obach R; Nin-Hill A; Bosch M; Palau M; Galindo A; Contreras S; Rovira A; Rovira C; Nonell S; Marchán V Redesigning the coumarin scaffold into small bright fluorophores with far-red to near-infrared emission and large Stokes shifts useful for cell imaging. *J. Org. Chem.* 2018, 83, 1185–1195. [PubMed: 29283264]
- (40). Schill H; Nizamov S; Bottanelli F; Bierwagen J; Belov VN; Hell SW 4-Trifluoromethyl-Substituted coumarins with large Stokes shifts: synthesis, bioconjugates, and their use in super-resolution fluorescence microscopy. *Chem. - Eur. J.* 2013, 19, 16556–16565. [PubMed: 24281806]
- (41). Nizamov S; Willig KI; Sednev MV; Belov VN; Hell SW Phosphorylated 3-heteroaryl coumarins and their use in fluorescence microscopy and nanoscopy. *Chem. - Eur. J.* 2012, 18, 16339–16348. [PubMed: 23111986]
- (42). Gorka AP; Nani RR; Schnermann MJ Harnessing cyanine reactivity for optical imaging and drug delivery. *Acc. Chem. Res.* 2018, 51, 3226–3235. [PubMed: 30418020]
- (43). Nani RR; Kelley JA; Ivanic J; Schnermann MJ Reactive species involved in the regioselective photooxidation of heptamethine cyanines. *Chem. Sci.* 2015, 6, 6556–6563. [PubMed: 26508998]
- (44). Byers GW; Gross S; Henrichs PM Direct and sensitized photooxidation of cyanine dyes. *Photochem. Photobiol.* 1976, 23, 37–43. [PubMed: 1265127]
- (45). Matikonda SS; Helmerich DA; Meub M; Beliu G; Kollmannsberger P; Greer A; Sauer M; Schnermann MJ Defining the basis of cyanine phototruncation enables a new approach to single-molecule localization microscopy. *ACS Cent. Sci.* 2021, 7, 1144–1155. [PubMed: 34345667]
- (46). Mofford DM; Reddy GR; Miller SC Latent luciferase activity in the fruit fly revealed by a synthetic luciferin. *Proc. Natl. Acad. Sci. U.S.A.* 2014, 111, 4443. [PubMed: 24616520]
- (47). Tinberg CE; Khare SD; Dou J; Doyle L; Nelson JW; Schena A; Jankowski W; Kalodimos CG; Johnsson K; Stoddard BL; Baker D Computational design of ligand-binding proteins with high affinity and selectivity. *Nature* 2013, 501, 212–216. [PubMed: 24005320]
- (48). Zanghellini A; Jiang L; Wollacott AM; Cheng G; Meiler J; Althoff EA; Röthlisberger D; Baker D New algorithms and an *in silico* benchmark for computational enzyme design. *Protein Sci.* 2006, 15, 2785–2794. [PubMed: 17132862]
- (49). Kuhlman B; Baker D Native protein sequences are close to optimal for their structures. *Proc. Natl. Acad. Sci. U.S.A.* 2000, 97, 10383–10388. [PubMed: 10984534]
- (50). Alford RF; Leaver-Fay A; Jeliakov JR; O'Meara MJ; DiMaio FP; Park H; Shapovalov MV; Renfrew PD; Mulligan VK; Kappel K; Labonte JW; Pacella MS; Bonneau R; Bradley P; Dunbrack RL; Das R; Baker D; Kuhlman B; Kortemme T; Gray JJ The Rosetta All-Atom Energy Function for Macromolecular Modeling and Design. *J. Chem. Theory Comput.* 2017, 13, 3031–3048. [PubMed: 28430426]
- (51). Cadwell RC; Joyce GF Mutagenic PCR. *Cold Spring Harb. Protoc.* 2006, 2006, No. pdb-prot4143.

- (52). Hosseinkhani S Molecular enigma of multicolor bioluminescence of firefly luciferase. *Cell. Mol. Life Sci.* 2011, 68, 1167–1182. [PubMed: 21188462]
- (53). Milne BF; Marques MAL; Nogueira F Fragment molecular orbital investigation of the role of AMP protonation in firefly luciferase pH-sensitivity. *Phys. Chem. Chem. Phys.* 2010, 12, 14285–14293. [PubMed: 20886161]
- (54). Viviani VR; Silva Neto AJ; Arnoldi FGC; Barbosa JARG; Ohmiya Y The influence of the loop between residues 223–235 in beetle luciferase bioluminescence spectra: a solvent gate for the active site of pH-sensitive luciferases. *Photochem. Photobiol.* 2008, 84, 138–144. [PubMed: 18173713]
- (55). Viviani VR; Oehlmeyer TL; Arnoldi FGC; Brochetto-Braga MR A new firefly luciferase with bimodal spectrum: identification of structural determinants of spectral pH-sensitivity in firefly luciferases. *Photochem. Photobiol.* 2005, 81, 843–848. [PubMed: 16124832]
- (56). Adamczyk M; Cornwell M; Huff J; Rege S; Rao TVS Novel 7-hydroxycoumarin based fluorescent labels. *Bioorg. Med. Chem. Lett.* 1997, 7, 1985–1988.
- (57). Naumov P; Ozawa Y; Ohkubo K; Fukuzumi S Structure and spectroscopy of oxyluciferin, the light emitter of the firefly bioluminescence. *J. Am. Chem. Soc.* 2009, 131, 11590–11605. [PubMed: 19722653]
- (58). Hall MP; Unch J; Binkowski BF; Valley MP; Butler BL; Wood MG; Otto P; Zimmerman K; Vidugiris G; Machleidt T; Robers MB; Benink HA; Eggers CT; Slater MR; Meisenheimer PL; Klaubert DH; Fan F; Encell LP; Wood KV Engineered luciferase reporter from a deep sea shrimp utilizing a novel imidazopyrazinone substrate. *ACS Chem. Biol.* 2012, 7, 1848–1857.
- (59). Liu S; Su Y; Lin MZ; Ronald JA Brightening up biology: advances in luciferase systems for *in vivo* imaging. *ACS Chem. Biol.* 2021, 16, 2707–2718. [PubMed: 34780699]
- (60). Nakayama J; Saito R; Hayashi Y; Kitada N; Tamaki S; Han Y; Semba K; Maki SA High sensitivity *in vivo* imaging of cancer metastasis using a near-infrared luciferin analogue seMpai. *Int. J. Mol. Sci.* 2020, 21, No. 7896. [PubMed: 33114327]
- (61). Amadeo F; Plagge A; Chacko A; Wilm B; Hanson V; Liptrott N; Murray P; Taylor A Firefly luciferase offers superior performance to AkaLuc for tracking the fate of administered cell therapies. *Eur. J. Nucl. Med. Mol. Imaging* 2022, 49, 796–808.
- (62). Yeh H-W; Karmach O; Ji A; Carter D; Martins-Green MM; Ai H-W Red-shifted luciferase-luciferin pairs for enhanced bioluminescence imaging. *Nat. Methods* 2017, 14, 971–974. [PubMed: 28869756]
- (63). Brennan CK; Yao Z; Ionkina AA; Rathbun CM; Sathishkumar B; Prescher JA Multiplexed bioluminescence imaging with a substrate unmixing algorithm. *Cell Chem. Biol.* 2022, 29, No. 1649.e4. [PubMed: 36283402]
- (64). Miller FR; Miller BE; Heppner GH Characterization of metastatic heterogeneity among subpopulations of a single mouse mammary tumor: heterogeneity in phenotypic stability. *Invasion Metastasis* 1983, 3, 22–31. [PubMed: 6677618]
- (65). McGranahan N; Swanton C Biological and therapeutic impact of intratumor heterogeneity in cancer evolution. *Cancer Cell* 2015, 27, 15–26. [PubMed: 25584892]
- (66). Siravegna G; Mussolin B; Buscarino M; Corti G; Cassingena A; Crisafulli G; Ponzetti A; Cremolini C; Amatu A; Lauricella C; Lamba S; Hobor S; Avallone A; Valtorta E; Rospo G; Medico E; Motta V; Antoniotti C; Tatangelo F; Bellosillo B; Veronese S; Budillon A; Montagut C; Racca P; Marsoni S; Falcone A; Corcoran RB; Di Nicolantonio F; Loupakis F; Siena S; Sartore-Bianchi A; Bardelli A Clonal evolution and resistance to EGFR blockade in the blood of colorectal cancer patients. *Nat. Med.* 2015, 21, 795–801. [PubMed: 26030179]
- (67). Schmidt F; Efferth T Tumor heterogeneity, single-cell sequencing, and drug resistance. *Pharmaceuticals* 2016, 9, 2. [PubMed: 26771619]
- (68). Marusyk A; Polyak K Tumor heterogeneity: Causes and consequences. *Biochim. Biophys. Acta, Rev. Cancer* 2010, 1805, 105–117.

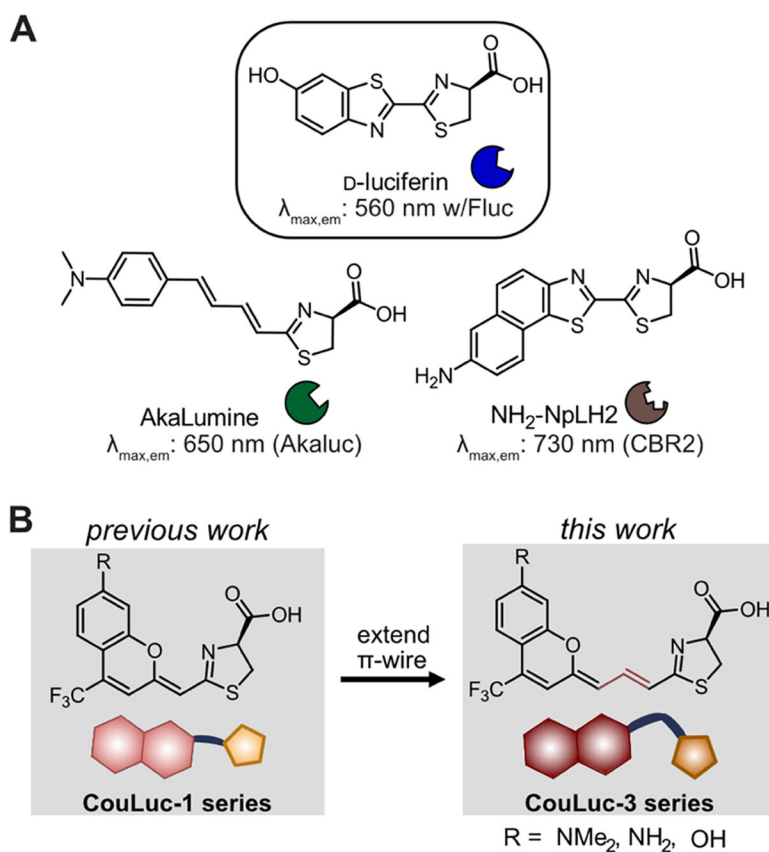


Figure 1. Red-shifted bioluminescent probe design. (A) Red-emitting analogues of D-luciferin. (B) First-generation coumarin luciferins (CouLuc-1 series) previously developed. The CouLuc-3 series featured in this work comprises an extra vinyl unit to redshift emission.

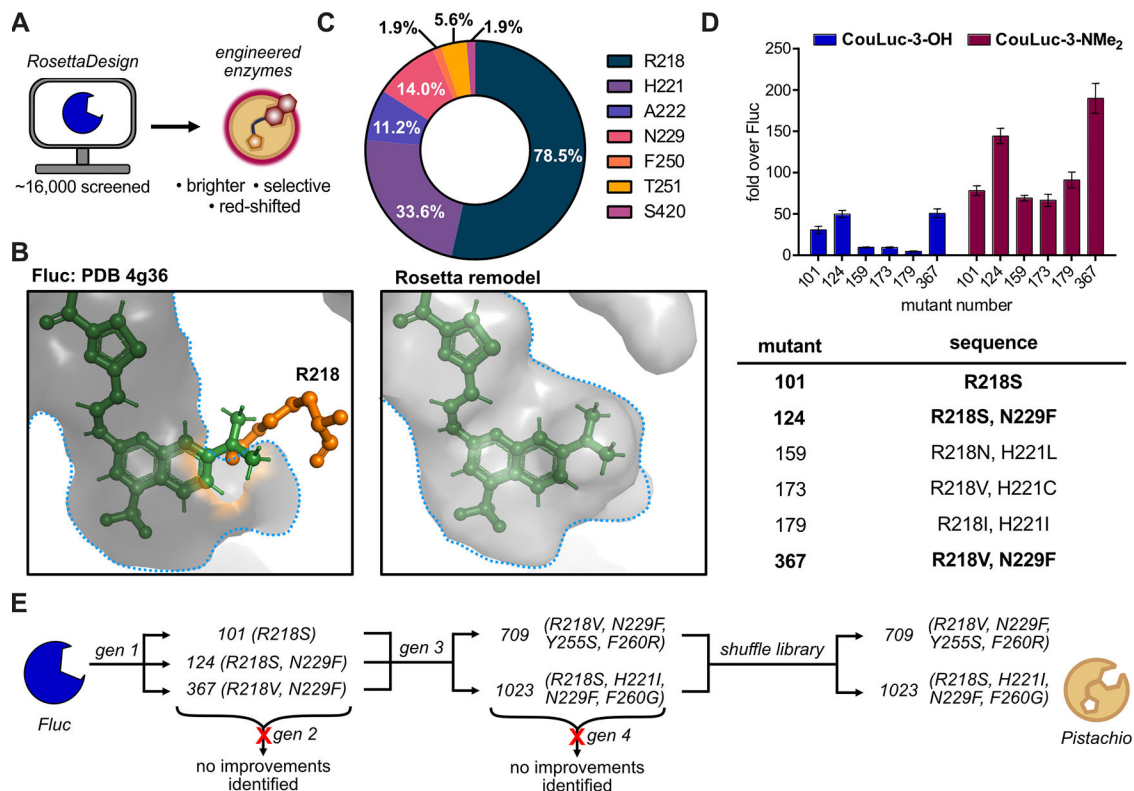
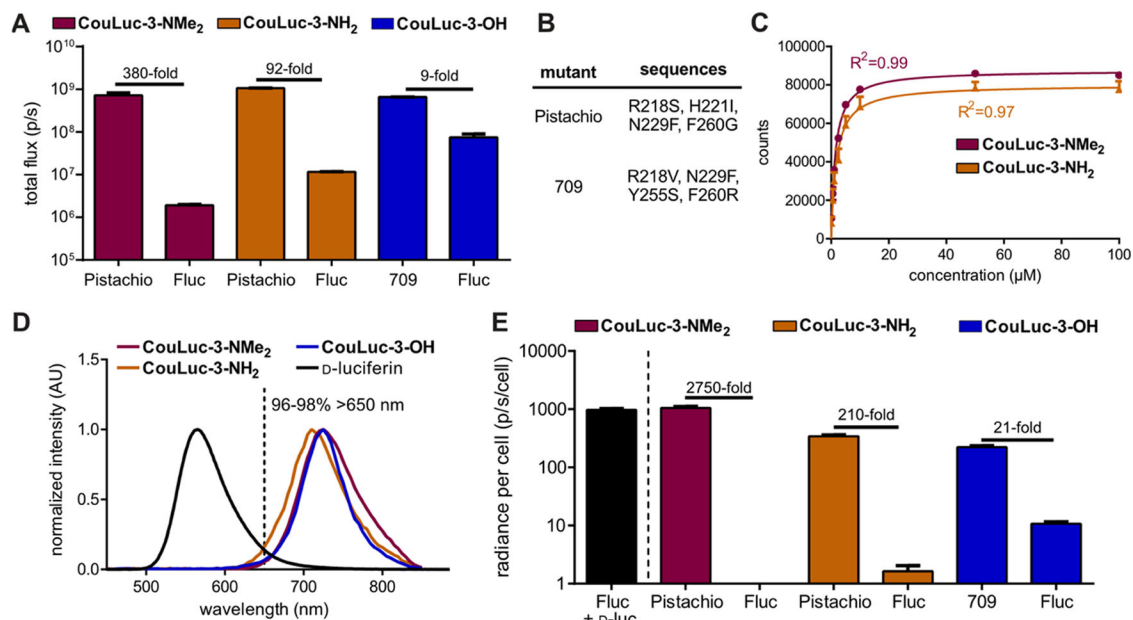


Figure 2. Searching for complementary luciferases via RosettaDesign. (A) Overall approach to identifying complementary luciferases for CouLuc-3 analogues. (B) Residue R218 was identified as a key site for mutagenesis in the generation 1 library. RosettaMatch docking revealed a steric clash between the electron-donating group and the arginine side chain. The blue dashed line indicates the binding pocket. (C) Percent abundance of residues mutated in top generation 1 hits. (D) Secondary screens identified several mutants displaying >100-fold improvements in emission over Fluc with the substrates. (E) Flowchart showing evolutionary progression toward top-performing mutants.

**Figure 3.**

Characterization of top mutant hits with CouLuc-3 analogues. (A) Improved light emission was observed when CouLuc-3 analogues (100 μM) were incubated with adenosine triphosphate (ATP, 1 mM), coenzyme A (1 mM), and recombinant luciferase mutants (Pistachio or 709). Emission intensities are plotted as total photon flux values. Error bars represent the standard error of the mean for $n = 3$ experiments. (B) Sequences of the top-performing mutants, Pistachio and 709. (C) Kinetic studies revealed amino CouLuc-3 analogues were more efficiently processed by Pistachio over Fluc (where no emission above background was observed). (D) Bioluminescence emission spectra of CouLuc-3 analogues. The luciferins (100 μM) were incubated with their respective top mutant hits (10 μM) at 25 °C. The emission spectrum of Fluc/D-luc is shown for comparison. (E) Improved photon outputs observed *in cellulo*. Pistachio/709- or Fluc-expressing cells were incubated with either a CouLuc-3 analogue (100 μM) or D-luc (100 μM). Peak emission intensities are plotted as photon flux per cell normalized to transfection efficiency and enzyme expression level (*via* co-expression of eGFP). Error bars represent the standard error of the mean for $n = 3$ experiments.

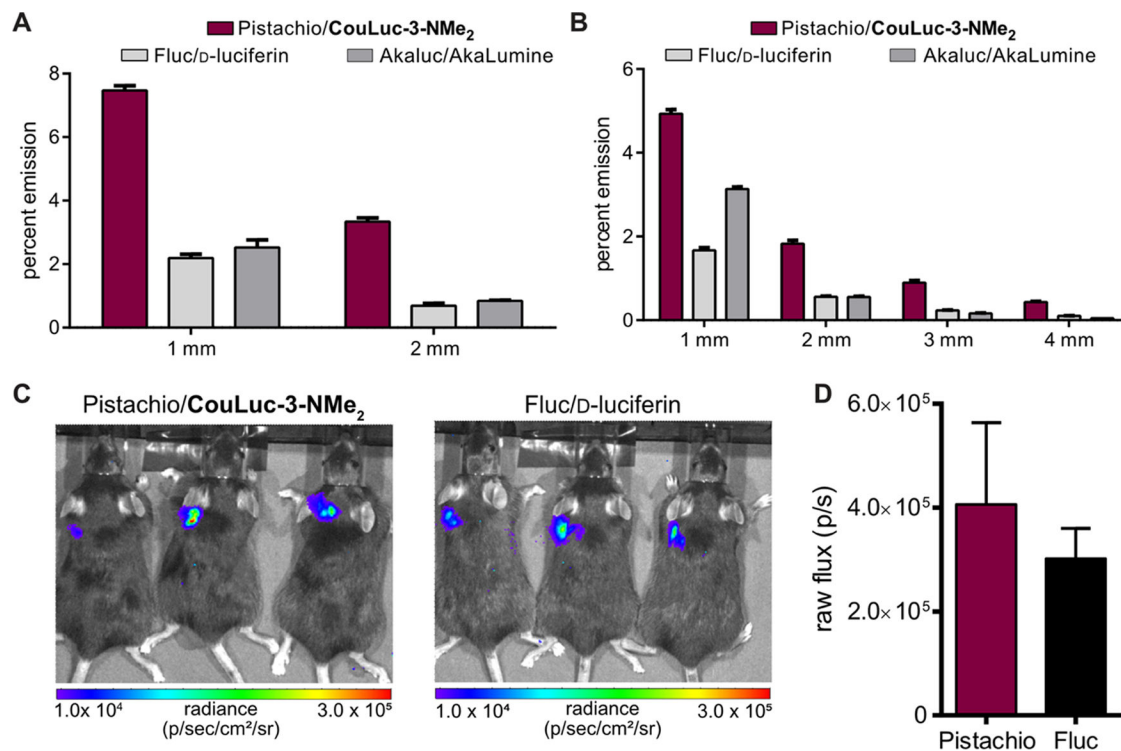


Figure 4.

Pistachio/CouLuc-3-NMe₂ is suitable for imaging in tissues. (A) 4T1 cells stably expressing Pistachio, Fluc, or Akaluc (5×10^4) were incubated with CouLuc-3-NMe₂, D-luciferin, or AkaLumine ($100 \mu\text{M}$), respectively. After acquisition of initial baseline images, individual slices of turkey bacon (Jenni-O, 1 mm thick) were layered on top of the wells containing cells with luciferin and images acquired after addition of each slice. Error bars represent the standard error of the mean for $n = 3$ experiments. (B) JIMT-1 cells stably expressing luciferase reporters were subjected to the same conditions as in (A). Due to higher luciferase expression in these cells, light emission was detected through four slices of bacon. Error bars represent the standard error of the mean for $n = 3$ experiments. (C) Bioluminescence imaging of JIMT-1 cells (1×10^5 cells per tumor) stably expressing either Pistachio-mRFP or Fluc-mRFP implanted in CL57BL/J6-scid mice. Tumors were grown for 4 days until just palpable (~ 1 mm diameter). The mice were injected i.p. with either formulated CouLuc-3-NMe₂ or D-luciferin (10 mM) and imaged over time. Representative peak emission data are shown. (D) Light output from Pistachio- and Fluc-expressing cells, measured at peak emission intensities and normalized for reporter expression levels. Error bars represent standard error of the mean for $n = 3$ samples.

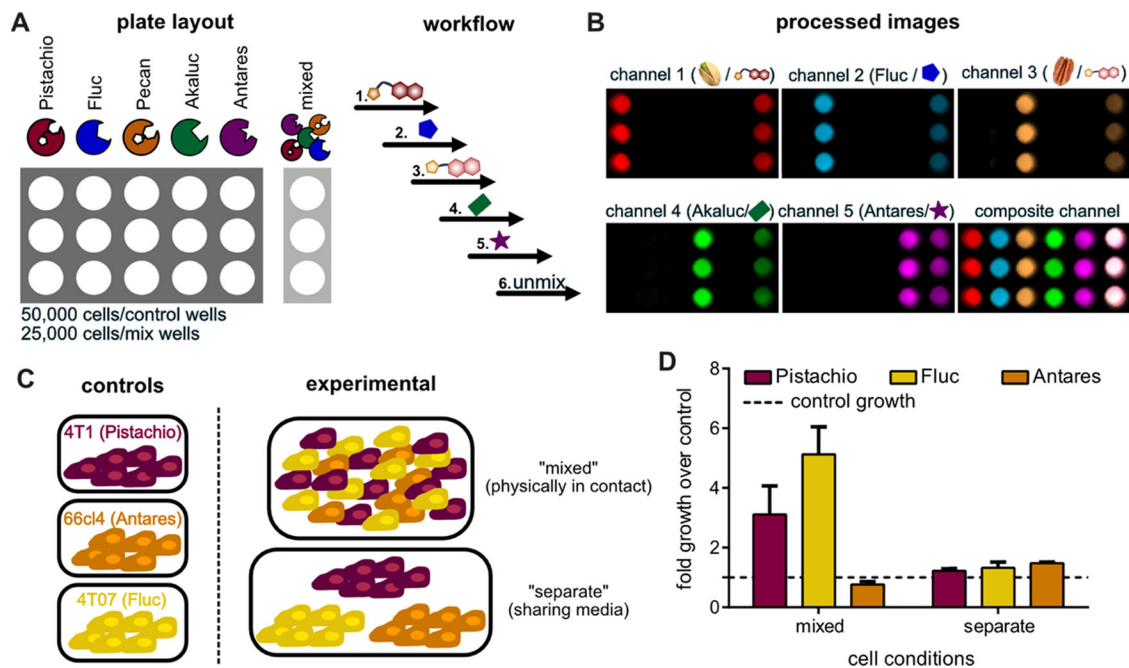
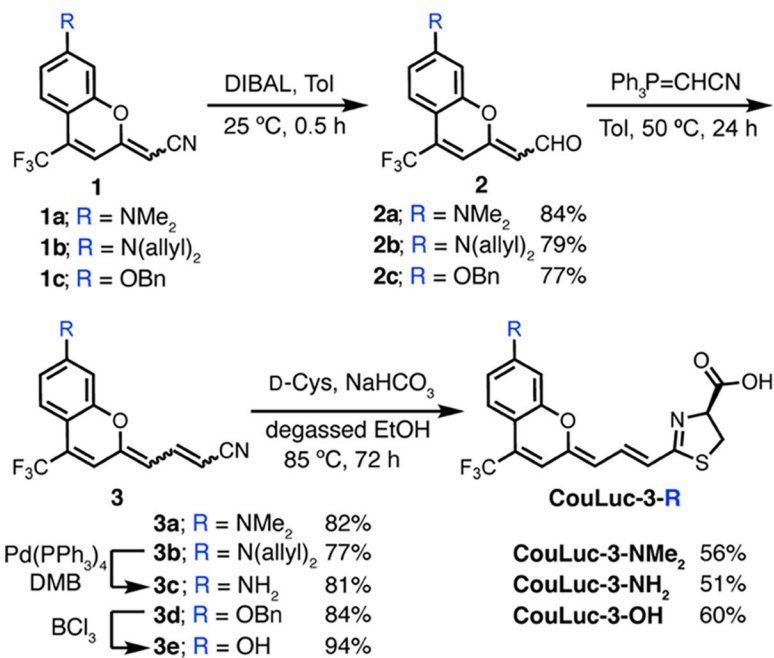


Figure 5.

Pistachio/CouLuc-3-NMe₂ can be synergized with other probes for multicomponent imaging. (A) JIMT-1 cells stably expressing either Pistachio-eGFP, Fluc-mRFP, Pecan-eGFP, Akaluc-TagBFP, or Antares were plated in single-culture wells (5×10^4) or mixed-culture conditions (2.5×10^4). Complementary luciferins were added to each well in the order shown, and raw images were subjected to linear unmixing analysis. (B) Processed images displaying orthogonality between selected luciferase/luciferin pairs. Data shown are representative of $n = 3$ biological replicates. (C) Cell lines stably expressing Pistachio-eGFP (4T1 parent line), Fluc-mRFP (4T07 parent line), or Antares (66cl4 parent line) were plated in distinct areas using biocompatible stencils. Cells were either plated alone (controls, 3×10^4) or together. Cells plated together were either mixed (1×10^4 cells per line per well) or separately (3×10^4), still allowing for media exchange. Stencils were removed, and cells were imaged over time. (D) Total flux values from the cultures were compared between day 1 and day 3 to determine differences in growth rates. The dotted line represents the growth rate for control cells (grown in isolation). Error bars represent the standard error of the mean for $n = 3$ experiments.



Scheme 1.
Synthesis of CouLuc-3 Series